NANO LETTERS

Letter

pubs.acs.org/NanoLett

Direct Growth of Single- and Few-Layer MoS_2 on h-BN with Preferred Relative Rotation Angles

Aiming Yan,[†,‡,∥] Jairo Velasco, Jr.,[†,∥] Salman Kahn,[†] Kenji Watanabe,[§] Takashi Taniguchi,[§] Feng Wang,[†,‡,∥] Michael F. Crommie,[†,‡,∥] and Alex Zettl*[,†,‡,∥]

[†]Department of Physics, University of California, Berkeley, California 94720, United States

[‡]Materials Sciences Division, Lawrence Berkeley National Laboratory, Berkeley, California 94720, United States

[§]National Institute for Materials Science, 1-1 Namiki, Tsukuba, 305-0044, Japan

[∥]Kavli Energy NanoSciences Institute at the University of California, Berkeley and the Lawrence Berkeley National Laboratory, Berkeley, California 94720, United States

Supporting Information

ABSTRACT: Monolayer molybdenum disulfide (MoS_2) is a promising two-dimensional direct-bandgap semiconductor with potential applications in atomically thin and flexible electronics. An attractive insulating substrate or mate for MoS_2 (and related materials such as graphene) is hexagonal boron nitride (h-BN). Stacked heterostructures of MoS_2 and h-BN have been produced by manual transfer methods, but a more efficient and scalable assembly method is needed. Here we demonstrate the direct growth of single- and few-layer MoS_2 on h-BN by chemical vapor deposition (CVD) method, which is scalable with suitably structured substrates. The growth mechanisms for single-layer and few-layer samples are found to be distinct, and for single-layer samples low relative rotation angles (<5°) between the MoS_2 and h-BN lattices prevail. Moreover, MoS_2 directly grown on h-BN maintains its intrinsic 1.89 eV bandgap. Our CVD synthesis method presents an important advancement toward controllable and scalable MoS_2-based electronic devices.

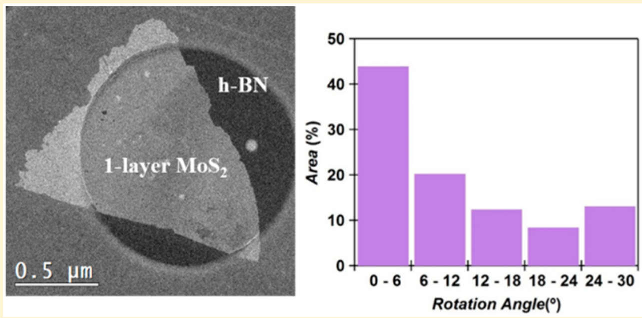

KEYWORDS: *Molybdenum disulfide, chemical vapor deposition, heterostructure, hexagonal boron nitride, screw-dislocation driven growth, transition metal dichalcogenides*

The realization of single-layer graphene on an insulating substrate[1] sparked renewed interest in van der Waals (vdW) bonded two-dimensional (2D) materials including the exploration of new phenomena and potential applications. Transition metal dichalcogenides (TMDs) are well-known vdW 2D structures that can also be exfoliated in single atomic layer form onto insulating substrates. Notably, TMDs display many physical properties distinct from those of graphene. MoS_2 is a particularly noteworthy TMD in that it displays a direct electronic bandgap of 1.89 eV in single layer form and a smaller indirect gap for multilayers. This transition allows much enhanced quantum yield of photoluminescence. Single-layer MoS_2-based field effect transistors (FETs) exhibit high on/off ratio[2] and control of valley polarization and coherence.[3] These properties establish MoS_2 as a promising candidate for flexible electronic, optoelectronic, and photonic applications.

Although for some applications suspended bare sheets of MoS_2 or other 2D materials is useful, in general the monolayers (or few layers) are mated to a substrate, either for mechanical stability or enhanced processability, or to create a desirable electronic/optical heterostructure. The mate is often a 2D vdW material itself, and fabricating heterostructures comprised of different 2D layered materials is a versatile approach that can integrate materials with different properties and realize new device functionalities.[4−6] Mating can be achieved through the manual transfer of individual 2D layered materials or the direct growth of one type of 2D material on top of or adjacent to another.[7,8] Although the transfer method enables virtually any combination of layered materials in a heterostructure, it is tedious and effectively nonscalable. Direct transfer can also trap impurities or residues at the interface between individual layers during the transfer.[6,9] In contrast, direct growth of a 2D layered material on top of or next to another is a more scalable and controllable method and yields clean interfaces.[7,8] Electrically insulating 2D h-BN has been shown to be a superior substrate to SiO_2/Si for graphene electronic devices due to the flat surface of h-BN and less charge inhomogeneity.[10−12] Similarly, it has also been shown that MoS_2 transferred onto h-BN exhibits excellent device quality.[13,14] The direct growth of MoS_2 on h-BN by CVD methods would be an important advance in

Received: April 3, 2015
Revised: August 18, 2015

DOI: 10.1021/acs.nanolett.5b01311
Nano Lett. XXXX, XXX, XXX−XXX

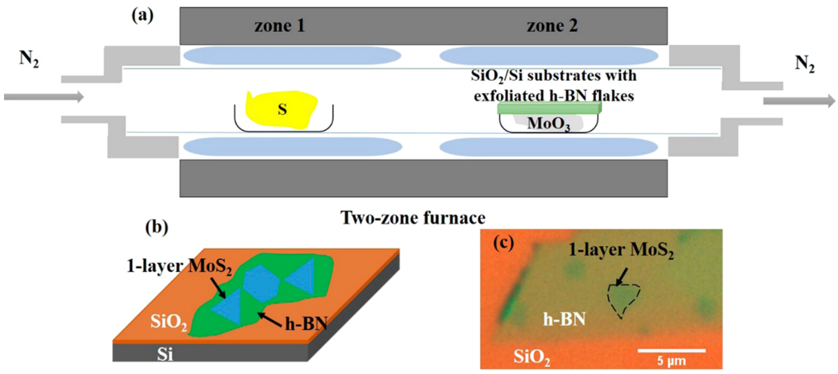

Figure 1. Experimental setup for the growth, schematic and optical image for representative samples from the growth. (a) Experimental setup for CVD growth of single- and few-layer MoS_2 on exfoliated h-BN. The quartz tube with S and MoO_3 precursors sits in the two-zone furnace. S is in zone 1 while MoO_3 precursor is in zone 2. Exfoliated h-BN flakes on SiO_2/Si chips are placed on top of the crucible that has MoO_3 precursor. N_2 gas runs through the quartz tube during the whole growth process; (b) Schematic of the geometry of as-grown single- and few-layer MoS_2 on exfoliated h-BN flakes, which are on a SiO_2/Si substrate. The green flakes represent thin h-BN (usually less than 200 nm thick) and blue flakes represent MoS_2 that have been grown on h-BN. (c) Optical image of a typical growth of MoS_2 islands on exfoliated thin h-BN flakes on SiO_2/Si substrates. The lighter green flakes are h-BN and the darker green regions are typical MoS_2 flakes. An MoS_2 flake is outlined in (c).

fabricating high-quality MoS_2 electronic devices in a scalable and controllable way.

CVD growth of MoS_2 on different substrates has been investigated extensively in the past two years.[15,16] With the seeding method, monolayer MoS_2 can be grown on various substrates[17,18] including h-BN.[18] However, growing MoS_2 directly on h-BN without any seeding method yields a clean interface between as-grown MoS_2 and h-BN substrate, which realizes the direct mating of these two layered materials. This not only allows the fabrication of higher-quality devices without extensive annealing processes, but also promotes interesting physics due to the direct coupling of MoS_2 and h-BN lattices. Here we demonstrate that single- and few-layer MoS_2 can be grown directly on exfoliated high-quality h-BN flakes using CVD. We find that the nominal growth mechanisms are different for single-layer and few-layer MoS_2. Single-layer samples display low relative rotation angles ($<5°$ with the specific definition for relative rotation angle discussed below) between the MoS_2 and h-BN hexagonal lattices.

Figure 1a shows the two-zone furnace setup for CVD growth of single- and few-layer MoS_2 on exfoliated h-BN on SiO_2/Si substrates. Unlike the reported one-zone furnace setup for the CVD growth of single-layer MoS_2 on bare SiO_2/Si substrates,[15,16] a two-zone furnace allows the separate control of S and MoO_3 sources and enables greater tunablility of the reaction process. The growth of single-layer MoS_2 on exfoliated h-BN is shown in the schematic in Figure 1b, where the green-colored flake represents h-BN exfoliated on a SiO_2/Si substrate and the isolated blue polygons represent single-layer MoS_2 flakes grown on the h-BN. Figure 1c is an optical image that depicts the typical end result of such a growth. The light green h-BN flakes are typically 20×10 μm^2 and the dark green MoS_2 islands have typical size 2−3 μm and are scattered randomly on the h-BN flake. On occasion, we also observe MoS_2 islands with higher optical contrast, suggesting growth of MoS_2 with layer number >1 is also possible (see below).

We examine the atomic-level topography of the MoS_2 islands on h-BN via atomic force microscopy (AFM), as shown in Figure 2. Three distinct MoS_2 island topographies are observed: (1) Flat and smooth MoS_2 islands (Figure 2a (ii),(iii)); (2) Flat and smooth MoS_2 islands that surround a tall protrusion at the center (Figure 2b (ii),(iii)); and (3) MoS_2 islands that exhibit striking helical fringes (Figure 2c (ii),(iii)).

We first focus on the (1) and (2) topographies because they are closely related; both represent single-layer MoS_2 growth and differ only in the size of the nucleation site. Both (1) and (2) topographies are usually isolated and located randomly on the h-BN flakes. A typical type (1) MoS_2 island is outlined with a blue box in Figure 2a (ii); Figure 2a (iii) shows a zoom-in of the boxed region. This MoS_2 island is ∼4 μm^2 in area, which is common for type (1) growth. Often, the MoS_2 islands of type (1) are polygon-shaped, while sometimes the grown single-layer MoS_2 flake can be striplike and can be as large as 10 μm^2 in area (Supporting Information Figure S1). A line profile from the edge of the MoS_2 island in Figure 2a (iii) is shown in Figure 2a (iv). The step edge profile reveals a height of ∼0.7 nm, consistent with the height of a single layer of MoS_2.[2,19] Although not revealed in Figure 2a, the likely nucleation site for the MoS_2 island in type (1) growth is a small defect in the h-BN, for example, a point vacancy.[20] The size and surface inhomogeneity (e.g., step edges) of h-BN flakes limit the size of single-layer MoS_2 that can be grown on h-BN. These two factors cause the discontinuity of single-layer MoS_2 growth in the lateral direction (see examples shown in Supporting Information Figures S1 and S2) and potentially cause inhomogeneous nucleation sites for MoS_2 to grow on h-BN.

In Figure 2b (ii), a flat and smooth MoS_2 island of topography (2), which surrounds a tall protrusion at the center, is outlined with a blue box. Figure 2b (iii) shows a zoom-in of the boxed region. MoS_2 islands of type (2) are typically flat and smooth with area 1−4 μm^2 and often have a flower petal-like shape. The tall protrusion in the center is usually smaller than 500 nm and has a polygon-like shape. Figure 2b (iv) and its inset shows an AFM line scan, consistent with single-layer MoS_2. The tall pillar-like protrusion in the center of the MoS_2 monolayer island is ∼25 nm tall and is itself composed of multilayer MoS_2. The pillar likely marks a rather drastic nucleation site in the underlying h-BN, such as a triangular multiatom defect[20,21] or impurities on the surface of h-BN. The growth of the single-layer islands of type (1) and (2) is depicted schematically in Figure 2a (i) and b (i).

With increased growth time, additional layers of MoS_2 can grow on top of the first layer of type (1) and (2) as discussed

DOI: 10.1021/acs.nanolett.5b01311
Nano Lett. XXXX, XXX, XXX−XXX

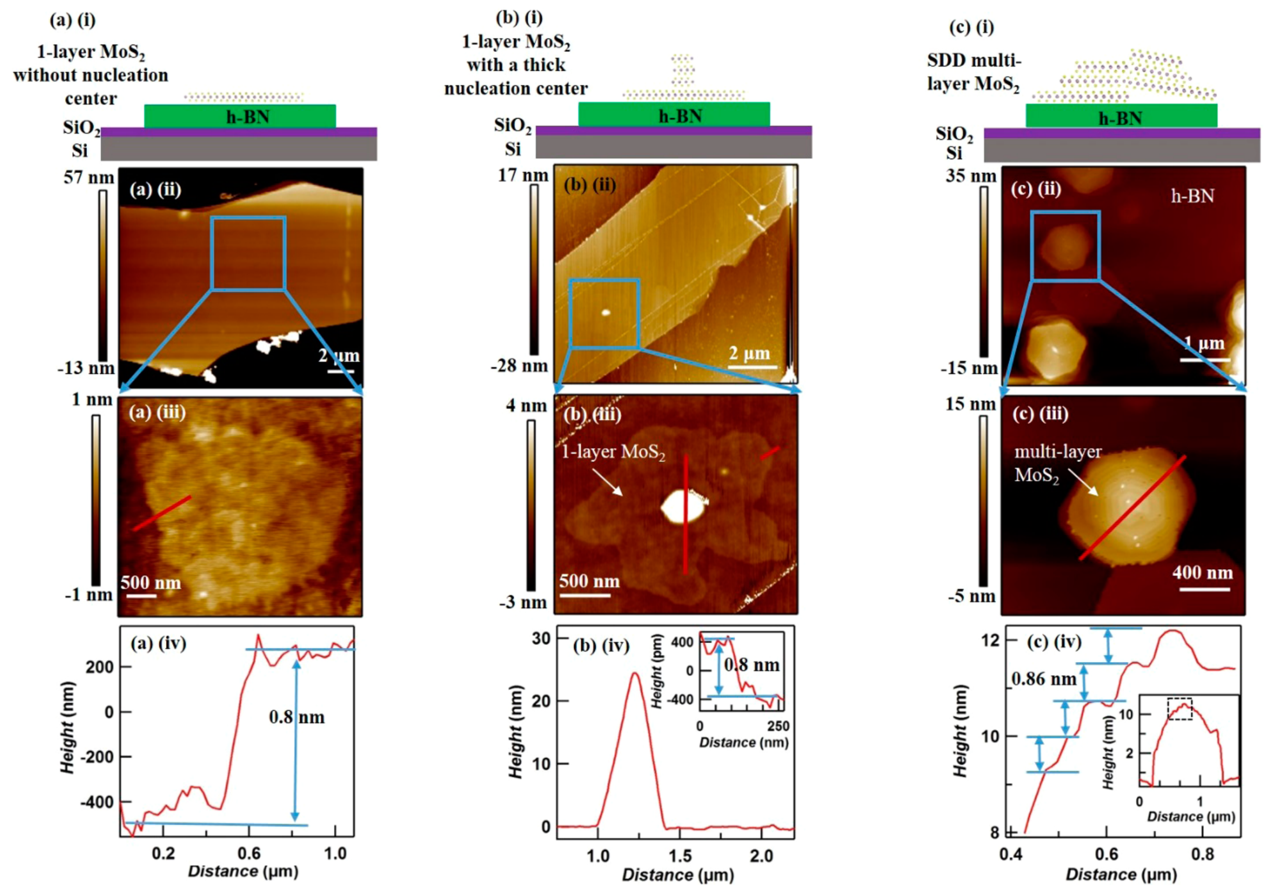

Figure 2. AFM characterization of single-layer and multilayer MoS_2 grown on exfoliated h-BN, which shows different growth mechanisms of MoS_2 on exfoliated h-BN by CVD method. (a,b) Both show the typical geometry of single-layer MoS_2 grown on h-BN. (a) A single-layer MoS_2 without a nucleation center can grow on h-BN. (a) (i) The schematic of such growth. The green slab represents an h-BN flake and the sandwich-structured MoS_2 is grown on top. (a) (ii) The low-magnification AFM image of single-layer MoS_2 on h-BN; (a) (iii) the zoom-in image of the area outlined by the blue box in a (ii). The height profile at the edge of MoS_2 shows the thickness is around 0.7 nm, which is consistent with single-layer MoS_2. (b) (i) The schematic for single-layer MoS_2 with a thick nucleation center. (b) (ii) The low-magnification AFM image of a single-layer MoS_2 with a thick nucleation center on h-BN; (b) (iii) the zoom-in image of the MoS_2 flake outlined in b (ii). Panel b (iii) shows the height profile across the nucleation center and the edge of MoS_2, showing the nucleation center is around 25 nm, while the edge shows a thickness of a single-layer MoS_2. (c) (i) The schematic for multilayer MoS_2 grown on h-BN. A typical multilayer MoS_2 island grown on h-BN follows the screw-dislocation-driven (SDD) growth mechanism. panel c (i) shows the growth starts from a screw-dislocation created at the interface of two MoS_2 flakes with one elementary burgers vector displaced vertically. (c) (ii) The low-magnification AFM image of a few multilayer MoS_2 islands grown on h-BN. (c) (iii) The zoom-in image of one MoS_2 island outlined in c (ii). The height profile across the center of MoS_2 island in (c) (iv) shows the step size of ~0.86 nm, which is about the thickness of one-layer MoS_2. The color scale for all the AFM images is adjusted so that as-grown MoS_2 flakes can be visualized from the contrast.

above and form multilayer MoS_2. One example is shown in Supporting Information Figure S2, where a smooth trilayer MoS_2 flake without an observable nucleation site is grown on h-BN. Multilayer MoS_2 obtained in this way follows so-called "layer-by-layer" ("LBL") growth mechanism.[22] This mechanism is typical for multilayer MoS_2[15,16] and other TMDs[8] grown by CVD method and is different from the screw-dislocation-driven (SDD) growth mechanism discussed later. An observable nucleation site that causes the type (2) single-layer MoS_2 growth sometimes will nucleate multilayer MoS_2 (typically 10 layers or less) over an extended region, much like the extended lower branches of a Christmas tree. An example is provided in Supporting Information Figure S3, where the as-grown multilayer MoS_2 is at an early stage of forming a Christmas tree shape. The growth of this type of multilayer MoS_2 with observable nucleation sites also follows "LBL" growth mechanism. However, based on our observation, smooth multilayer MoS_2 flakes grown on h-BN rarely show observable nucleation sites.

Figure 2c (ii) shows an example of topography (3), which is distinct from topographies (1) and (2): the MoS_2 islands are pyramid-like with hexagonal or triangular bases. The type (3) islands are of different maximum thickness and are located randomly on the h-BN flakes. Interestingly, the type (3) islands have a helical (spiral) structure in the normal direction. Figure 2c (iii) shows a zoom-in image of one of the islands, and Figure 2c (iv) shows the result of an AFM line scan acquired along the red line of Figure 2c (iii). The entire island structure identified here has a height of ~10 nm and steplike features with 0.86 nm heights. This clearly represents multilayer MoS_2, grown in a screw-like manner.

Topography (3) multilayer MoS_2 islands result from a screw-dislocation-driven (SDD) growth mechanism. This has also been observed in other CVD grown TMD materials[23,24] and has been attributed to a low supersaturation condition. The

DOI: 10.1021/acs.nanolett.5b01311
Nano Lett. XXXX, XXX, XXX−XXX

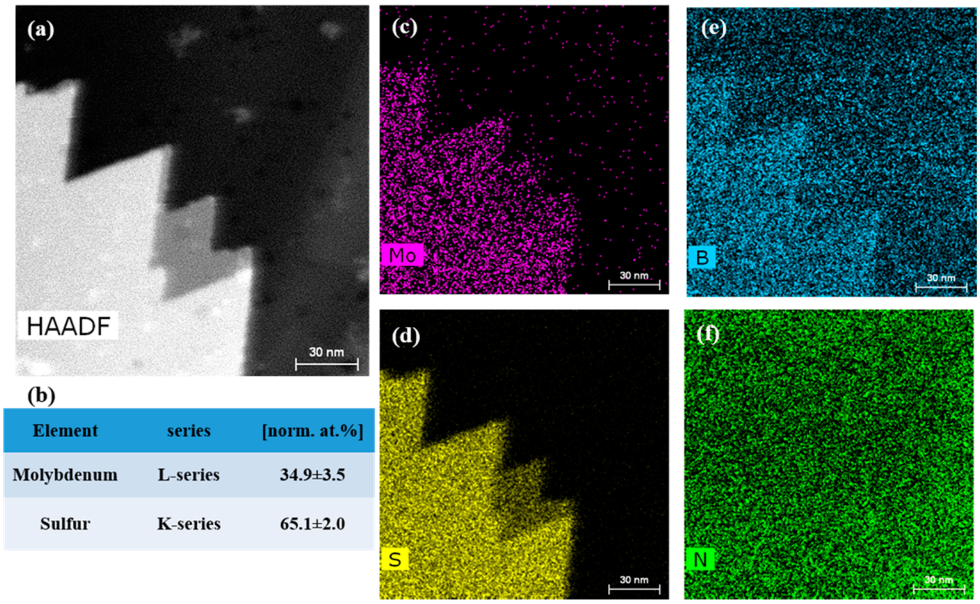

Element	series	[norm. at.%]
Molybdenum	L-series	34.9±3.5
Sulfur	K-series	65.1±2.0

Figure 3. STEM EDS mapping of thin MoS_2 grown on exfoliated h-BN, showing the composition/stoichiometry of MoS_2 flakes on h-BN. (a) High-angle annular dark-field (HAADF) image of few-layer MoS_2 on h-BN. The white region is as-grown thin MoS_2 while the dark background is h-BN. (c−f) The elemental maps of MoS_2 on h-BN, showing the location of Mo, S, B and N respectively. The Mo and S maps clearly show the MoS_2 flake. N map shows uniform distribution while B map shows higher intensity around the location of the MoS_2 flake. The nonuniform distribution of B is due to the overlap of the B and Mo peaks in the spectrum (Supporting Information Figure S5); the concentration of B is based on the intensity of the B peak around 0.18 keV and this B peak may include some intensity from the Mo peak located around the same energy. (b) The atomic composition of Mo (34.9 ± 3.5%) and S (65.1 ± 2.0%), analyzed from the STEM EDS mapping. The atomic ratio between Mo and S is close to the expected 1:2 for MoS_2.

SDD growth mechanism is also a common growth mode observed in other anisotropic nanostructure growths.[25−28] We depict this growth in Figure 2c (i) as a cross-sectional schematic of multilayer MoS_2 grown on h-BN. For SDD growth of a 2D material, the starting point is typically a vertical offset (or slip) in the atomic planes of the first growth layer. Once the screw dislocation is created, the following layers tend to nucleate and grow from the exposed edge of the dislocation due to the decreased energy barrier at these sites, which promotes more vertical growth than lateral growth. Both the helical features and the profile with a step height of 0.86 nm, which is close to the thickness of single-layer MoS_2, indicate the type (3) multilayer islands of MoS_2 represent SDD growth with a single elementary Burgers vector for the screw dislocation.[23,29] We have also observed herringbone contours (Supporting Information Figure S4) in few-layer MoS_2 grown on h-BN, which are typical features in SDD growth.[23,29] An identifying feature of this growth mechanism is an extended offset in height corresponding to the Burgers vector of the screw dislocation (or a slipped edge).[23,24,28] Because our AFM scans of as-grown single-layer MoS_2 on h-BN did not show this identifying feature, we conclude the SDD growth mechanism does not produce single-layer MoS_2 in our case.

Here we summarize the growth mechanisms for single-layer and multilayer MoS_2 grown on h-BN. Smooth single-layer MoS_2 can grow on h-BN with or without observable nucleation sites, while smooth multilayer MoS_2 can grow on h-BN following "LBL" growth mechanism, which is an extension of smooth single-layer MoS_2 growth. Multilayer MoS_2 can also nucleate and grow on h-BN from a screw dislocation, which is called SDD growth mechanism.

We employ transmission electron microscopy (TEM) to further characterize MoS_2 grown on h-BN. Figure 3a shows for a type (2) multilayer MoS_2 island the high-angle-annular-dark-field (HAADF) image. Because MoS_2 is atomically heavier than h-BN the HAADF image will show significant contrast between MoS_2 and h-BN. Indeed, in Figure 3a we observe a bright triangular area on top of a distinct dark background, representing the presence of MoS_2 on h-BN. Energy-dispersive X-ray spectroscopy (EDS) mapping with distributions of Mo, S, B, and N are also shown in Figure 3b−e, respectively. In this EDS mapping, B and N are found in the entire area indicating h-BN is present everywhere within the observation window, as expected. Mo and S are distributed in a manner similar to the shape of the bright contrast in Figure 3a and are clearly attributed to MoS_2. EDS analysis also allows the Mo/S ratio to be determined; we find 34.9 ± 3.5 to 65.1 ± 2.0, consistent (considering experimental uncertainties) with the expected composition 1:2 for MoS_2. Our TEM EDS measurements thus unambiguously confirm the flakes grown in this study as MoS_2.

To characterize the quality of monolayer MoS_2 crystals grown on h-BN, we perform photoluminescence (PL) experiments (Figure 4), and compare the results to PL measurements on single-layer MoS_2 grown on SiO_2 via CVD. AFM is used to ensure that the MoS_2 samples are single layer. Our single-layer MoS_2 grown on h-BN has a strong PL peak centered at 1.89 eV (Figure 4). This measured direct band gap is quite close to the one of free-standing exfoliated single-layer MoS_2- 1.90 eV,[30] and is larger than the CVD grown MoS_2 on SiO_2 (1.84 eV[15]) and exfoliated single-layer MoS_2 on SiO_2 (1.85 eV[31]). The full width at half-maximum (FWHM) of the PL peak from as-grown MoS_2/h-BN heterostructure is approximately 40 meV, which is slightly smaller than that for CVD grown MoS_2 on SiO_2 (50 meV) as shown in Figure 4 and also in reference[15] and free-standing exfoliated MoS_2 (50−60 meV[30]), and is much smaller than MoS_2 exfoliated onto SiO_2

DOI: 10.1021/acs.nanolett.5b01311
Nano Lett. XXXX, XXX, XXX−XXX

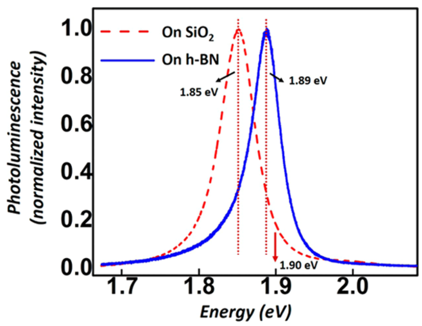

Figure 4. Photoluminescence from single-layer MoS_2 grown on h-BN. Photoluminescence peak from single-layer MoS_2 grown on h-BN (1.89 eV) indicates a band gap closer to free-standing MoS_2 flake (1.90 eV, pointed out by the arrow) compared to that grown on SiO_2 (1.85 eV).

(100- 150 meV[31]). These characteristics of PL indicate that MoS_2 grown on h-BN is electronically less perturbed than that grown on SiO_2, and is more like free-standing MoS_2. We note, the high growth temperature can cause stretching of as-grown MoS_2 after the sample cools down to room temperature, due to h-BN's negative lateral thermal expansion coefficient and MoS_2's positive lateral thermal expansion coefficient. The photoluminescence peak from stretched single-layer MoS_2 will red-shift compared to single-layer MoS_2 grown on SiO_2.[32] However, the photoluminescence peak from single-layer MoS_2 grown on h-BN studied here was consistently observed to be close to the peak from free-standing monolayer MoS_2, and blue-shifted compared to MoS_2 grown on SiO_2. Thus, the effect of the electrical environment for MoS_2 grown on h-BN is greater than the influence from strain effects. This supports our claim that MoS_2 grown on h-BN is less electrically disturbed, which is consistent with studies on single-layer MoS_2 transferred onto h-BN.[13,14]

We now turn to the relative crystal orientation of MoS_2 grown on h-BN. The relative rotation angle between the constituent layers in a 2D heterostructure can play a significant role in the electronic band structure of the heterostructure.[7,33,34] Although MoS_2 and h-BN both exhibit hexagonal crystal structure, the associated lattice constants differ by >20% and are incommensurate; hence it is *a priori* unclear if any preferred orientation between MoS_2 and h-BN lattices should occur. We find, however, that there is a strong orientation preference.

We examine a dilute collection of independent, nearly identical small (~500 nm) triangular crystallites of MoS_2 grown on single-crystal h-BN, and observe two highly dominant relative orientations, differing by 60° (Supporting Information Figure S7). We use selected area electron diffraction (SAED) in TEM to confirm the absolute orientation angles: the peaks in the bimodal distribution indeed correspond to crystal lattices' alignment, with the orientation of "S" sublattice of MoS_2 aligned with either the "B" sublattice or the "N" sublattice of h-BN, with equal probability. In other words, the orientation of MoS_2 is sensitive to the atomic corrugation of h-BN but it does not appreciably distinguish between B and N atoms. In our detailed SAED analysis below, we exploit this indistinguishability and conveniently employ a reduced angle definition for the relative orientation angle (see Supporting Information Figure S6), where the reduced misorientation angle spans 0°−30°.

We focus for the moment on single-layer MoS_2 grown on h-BN and employ SAED to characterize the rotation angle for 22 MoS_2 overlayers. Figure 5a shows a typical SAED pattern in which there are two sets of six-fold symmetric diffraction spots. The six spots of the inner hexagon (denoted by green lines) correspond to MoS_2 (a_{MoS_2} = 3.1 Å) and the six spots of the outer hexagon (denoted by purple lines) correspond to h-BN ($a_{h\text{-}BN}$ = 2.5 Å). From this pattern we measure a relative rotation angle between MoS_2 and h-BN of ~9°. By selecting one diffraction spot of MoS_2, one can visualize the MoS_2 flake in dark-field image (Figure 5b), where MoS_2 appears bright and the dark background is h-BN. On the basis of the area probability histogram for specific relative rotation angles between the as-grown single-layer MoS_2 and h-BN (from 22 locations), a low angle (<6°) is most dominant (around 45% area fraction), as shown in Figure 5c. The histogram for counts also shows that 10 out of 22 single-layer MoS_2 flakes grown on h-BN have relative rotation angles <6° (Figure 5d). Single-layer MoS_2 flakes that have a relative rotation angle 6°−12° and 24°−30° are also present but are less prevalent.

The preferred low relative rotation angles between MoS_2 and h-BN can be attributed to van der Waals epitaxy[35] that is modified by several factors. van der Waals epitaxy permits one type of 2D material to grow on another type in a rotationally commensurate manner, despite the highly mismatched lattice constants of the constituent materials. The slightly broadened distribution in rotation angle (within 6° range) in our MoS_2/h-BN heterostructure suggests additional factors play a role in deviation from van der Waals epitaxy. This has also been observed in previous studies of other directly grown TMDs on various substrates.[36,37]

The study of relative rotation angle between multilayer MoS_2 and the h-BN substrate is less straightforward due to the more complex growth mechanism of multilayer MoS_2 islands grown on h-BN compared to the single-layer MoS_2 case. In this case, we often observe multiple relative rotation angles although the h-BN substrate may be one single-crystal domain. Figure 5e shows a triangular MoS_2 thick island grown on h-BN. The significant contrast at the center of the MoS_2 flake is caused by the screw-dislocation. The SAED pattern taken from the outlined area in Figure 5e is shown in Figure 5f. There are at least two relative rotation angles in Figure 5f, but one strongly apparent and symmetric set of diffraction spots from MoS_2 shows the relative rotation angle is 3°, which is consistent with the most probable relative rotation angle for single-layer MoS_2 grown on h-BN as shown in Figure 5c,d.

In summary, we have demonstrated that single-layer and few-layer MoS_2 can be directly grown on h-BN by CVD method. The growth mechanisms were found to differ depending on the different supersaturation condition of precursors. Under low supersaturation condition, screw-dislocation-driven growth dominates and causes the few-layer MoS_2 to form striking helical structures. Otherwise, smooth single-layer and few-layer MoS_2 with nonobservable or observable nucleation centers can form on h-BN, following "layer-by-layer" growth mechanism. The as-grown single-layer MoS_2 on h-BN shows a strong photoluminescence peak centered around 1.89 eV, which is closer to that of free-standing MoS_2. This indicates single-layer MoS_2 grown on h-BN has less perturbed electrical environment and is promising for high-quality MoS_2-based devices. Detailed TEM studies show that single-layer MoS_2 grown on h-BN has preferred low relative rotation angle between the two, which is

DOI: 10.1021/acs.nanolett.5b01311
Nano Lett. XXXX, XXX, XXX−XXX

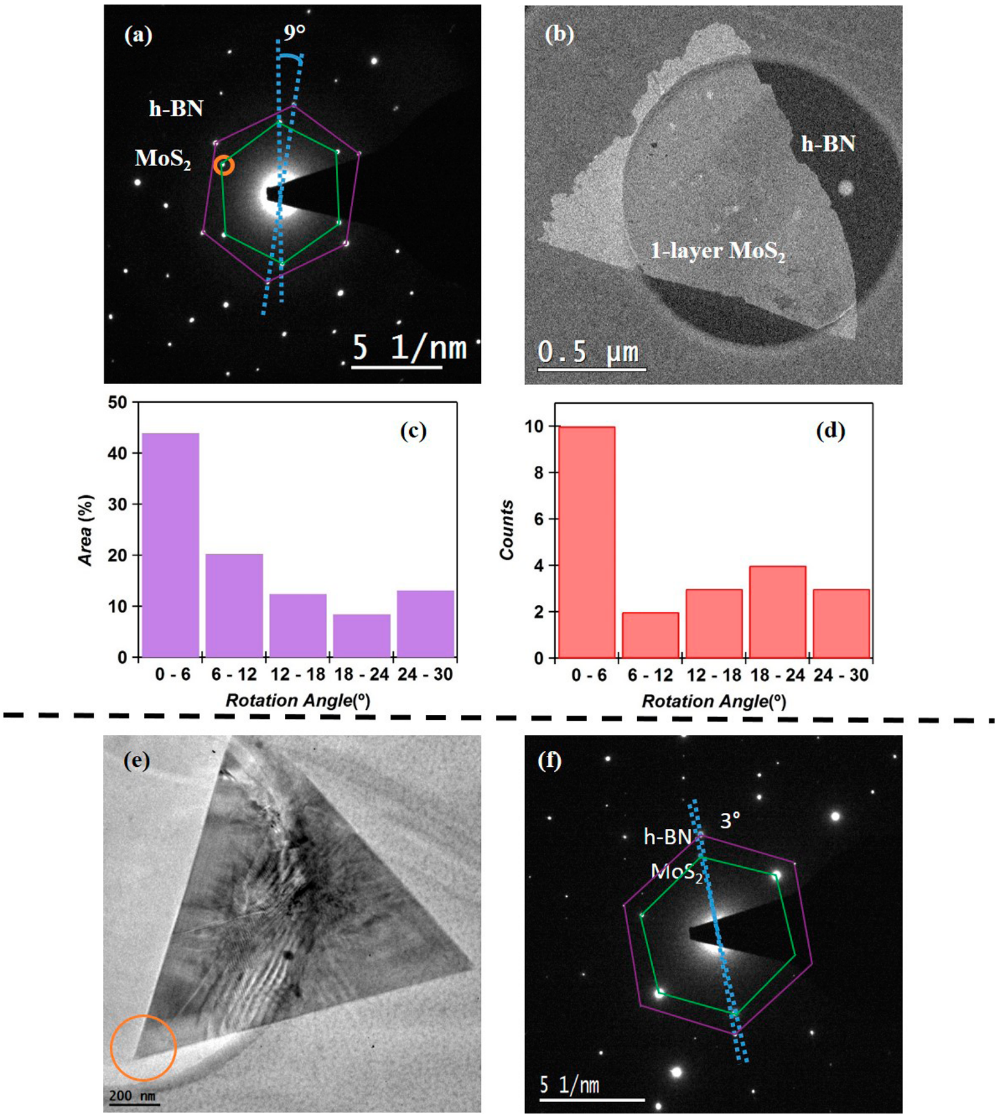

Figure 5. TEM characterization of single-layer and multilayer MoS_2 grown on exfoliated h-BN. (a) A typical selected area electron diffraction (SAED) pattern of a single-layer MoS_2 flake grown on thin h-BN. The green hexagon shows the six-fold-symmetric diffraction spots from MoS_2 while the purple hexagon shows the six-fold-symmetric diffraction spots from h-BN. The relative rotation angle between MoS_2 and h-BN is measured to be 9° from this diffraction pattern. By selecting one of the diffraction spots from MoS_2 (outlined in (a)), one can visualize the MoS_2 flake in dark filed image shown in (b). The white region in (b) is the single-layer MoS_2 while h-BN appears dark. The white dot visible on h-BN is residual polymer from TEM sample preparation, which also indicates the dark region is not empty. The heterostructure of MoS_2 and h-BN lies over a hole on a quantifoil TEM grid. (c) shows the area probability histogram of the relative rotation angle of single-layer MoS_2 grown on h-BN based on 22 locations of such growth. (d) The count histogram of the same growths in (c). (e) A TEM image of a typical triangular multilayer MoS_2 island grown on h-BN. The contrast due to the screw dislocation is visible around the center of MoS_2 island. (f) The diffraction pattern from the region outlined in (d). The green hexagon outlines the diffraction spots from MoS_2 while the purple hexagon outlines the diffraction spots from h-BN. The relative rotation angle between MoS_2 and h-BN at this specific location is ∼3°.

also interesting for further study of electronic band structure modification due to different relative rotation angle in this heterostructure.

After submission of this work, we became aware of a related independent report[38] of MoS_2 grown directly on CVD prepared h-BN (which had been transferred to SiO_2 substrates for MoS_2 growth).

■ ASSOCIATED CONTENT

Supporting Information

The Supporting Information is available free of charge on the ACS Publications website at DOI: 10.1021/acs.nanolett.5b01311.

Materials and Methods and Figures S1 to S7. (PDF)

■ AUTHOR INFORMATION

Corresponding Author

*E-mail: azettl@berkeley.edu.

Notes

The authors declare no competing financial interest.

■ ACKNOWLEDGMENTS

This research was supported in part by the Director, Office of Basic Energy Sciences, Materials Sciences and Engineering Division of the U.S. Department of Energy under Contract DE-

AC02-05CH11231 within the sp2-bonded Materials Program, which provided for postdoctoral support and AFM and PL characterization; by NSF Grant DMR-1206512, which provided for the sample growth, and by the Molecular Foundry of the Lawrence Berkeley National Laboratory, under Contract DE-AC02-05CH11231, which provided for TEM characterization. We acknowledge Karen Bustillo in the Molecular Foundry of the Lawrence Berkeley National Laboratory for TEM technical support and Dr. Wei Chen in the Electrochemical Technologies Group of the Lawrence Berkeley National Laboratory for useful discussion. Illuminating discussions with Ashley Gibb are also acknowledged.

■ REFERENCES

(1) Novoselov, K. S.; Geim, A. K.; Morozov, S. V.; Jiang, D.; Zhang, Y.; Dubonos, S. V.; Grigorieva, I. V.; Firsov, A. A. Electric Field Effect in Atomically Thin Carbon Films. *Science (Washington, DC, U. S.)* **2004**, *306*, 666−669.

(2) Radisavljevic, B.; Radenovic, A.; Brivio, J.; Giacometti, V.; Kis, A. Single-Layer MoS2 Transistors. *Nat. Nanotechnol.* **2011**, *6*, 147−150.

(3) Xu, X.; Yao, W.; Xiao, D.; Heinz, T. F. Spin and Pseudospins in Layered Transition Metal Dichalcogenides. *Nat. Phys.* **2014**, *10*, 343−350.

(4) Wang, L.; Meric, I.; Huang, P. Y.; Gao, Q.; Gao, Y.; Tran, H.; Taniguchi, T.; Watanabe, K.; Campos, L. M.; Muller, D. A.; et al. One-Dimensional Electrical Contact to a Two-Dimensional Material. *Science* **2013**, *342*, 614−617.

(5) Mayorov, A. S.; Gorbachev, R. V.; Morozov, S. V.; Britnell, L.; Jalil, R.; Ponomarenko, L. A.; Blake, P.; Novoselov, K. S.; Watanabe, K.; Taniguchi, T.; et al. Micrometer-Scale Ballistic Transport in Encapsulated Graphene at Room Temperature. *Nano Lett.* **2011**, *11*, 2396−2399.

(6) Kretinin, A. V.; Cao, Y.; Tu, J.-S.; Yu, G.; Jalil, R.; Novoselov, K. S.; Haigh, S.; Gholinia, A.; Mishchenko, A.; Lozada, M.; et al. Electronic Properties of Graphene Encapsulated with Different 2D Atomic Crystals. *Nano Lett.* **2014**, *14*, 3270−3276.

(7) Yang, W.; Chen, G.; Shi, Z.; Liu, C.-C.; Zhang, L.; Xie, G.; Cheng, M.; Wang, D.; Yang, R.; Shi, D.; et al. Epitaxial Growth of Single-Domain Graphene on Hexagonal Boron Nitride. *Nat. Mater.* **2013**, *12*, 792−797.

(8) Gong, Y.; Lin, J.; Wang, X.; Shi, G.; Lei, S.; Lin, Z.; Zou, X.; Ye, G.; Vajtai, R.; Yakobson, B. I.; et al. Vertical and in-Plane Heterostructures from WS2/MoS2Monolayers. *Nat. Mater.* **2014**, *13*, 1135−1142.

(9) Haigh, S. J.; Gholinia, A.; Jalil, R.; Romani, S.; Britnell, L.; Elias, D. C.; Novoselov, K. S.; Ponomarenko, L. A.; Geim, A. K.; Gorbachev, R. Cross-Sectional Imaging of Individual Layers and Buried Interfaces of Graphene-Based Heterostructures and Superlattices. *Nat. Mater.* **2012**, *11*, 764−767.

(10) Dean, C. R.; Young, A. F.; Meric, I.; Lee, C.; Wang, L.; Sorgenfrei, S.; Watanabe, K.; Taniguchi, T.; Kim, P.; Shepard, K. L.; et al. Boron Nitride Substrates for High-Quality Graphene Electronics. *Nat. Nanotechnol.* **2010**, *5*, 722−726.

(11) Xue, J.; Sanchez-Yamagishi, J.; Bulmash, D.; Jacquod, P.; Deshpande, A.; Watanabe, K.; Taniguchi, T.; Jarillo-Herrero, P.; LeRoy, B. J. Scanning Tunnelling Microscopy and Spectroscopy of Ultra-Flat Graphene on Hexagonal Boron Nitride. *Nat. Mater.* **2011**, *10*, 282−285.

(12) Decker, R.; Wang, Y.; Brar, V. W.; Regan, W.; Tsai, H.-Z.; Wu, Q.; Gannett, W.; Zettl, A.; Crommie, M. F. Local Electronic Properties of Graphene on a BN Substrate via Scanning Tunneling Microscopy. *Nano Lett.* **2011**, *11*, 2291−2295.

(13) Lee, G.-H.; Yu, Y.-J.; Cui, X.; Petrone, N.; Lee, C.-H.; Choi, M. S.; Lee, D.-Y.; Lee, C.; Yoo, W. J.; Watanabe, K.; et al. Flexible and Transparent MoS2 Field-Effect Transistors on Hexagonal Boron Nitride-Graphene Heterostructures. *ACS Nano* **2013**, *7*, 7931−7936.

(14) Cui, X.; Lee, G.-H.; Kim, Y. D.; Arefe, G.; Huang, P. Y.; Lee, C.-H.; Chenet, D. A.; Zhang, X.; Wang, L.; Ye, F.; et al. Multi-Terminal Transport Measurements of MoS2 Using a van Der Waals Heterostructure Device Platform. *Nat. Nanotechnol.* **2015**, *10*, 534−540.

(15) Van der Zande, A. M.; Huang, P. Y.; Chenet, D. A.; Berkelbach, T. C.; You, Y.; Lee, G.-H.; Heinz, T. F.; Reichman, D. R.; Muller, D. A.; Hone, J. C. Grains and Grain Boundaries in Highly Crystalline Monolayer Molybdenum Disulphide. *Nat. Mater.* **2013**, *12*, 554−561.

(16) Najmaei, S.; Liu, Z.; Zhou, W.; Zou, X.; Shi, G.; Lei, S.; Yakobson, B. I.; Idrobo, J.-C.; Ajayan, P. M.; Lou, J. Vapour Phase Growth and Grain Boundary Structure of Molybdenum Disulphide Atomic Layers. *Nat. Mater.* **2013**, *12*, 754−759.

(17) Lee, Y.-H.; Zhang, X.-Q.; Zhang, W.; Chang, M.-T.; Lin, C.-T.; Chang, K.-D.; Yu, Y.-C.; Wang, J. T.-W.; Chang, C.-S.; Li, L.-J.; et al. Synthesis of Large-Area MoS2 Atomic Layers with Chemical Vapor Deposition. *Adv. Mater.* **2012**, *24*, 2320−2325.

(18) Ling, X.; Lee, Y.-H.; Lin, Y.; Fang, W.; Yu, L.; Dresselhaus, M. S.; Kong, J. Role of the Seeding Promoter in MoS2 Growth by Chemical Vapor Deposition. *Nano Lett.* **2014**, *14*, 464−472.

(19) Novoselov, K. S.; Jiang, D.; Schedin, F.; Booth, T. J.; Khotkevich, V. V.; Morozov, S. V.; Geim, A. K. Two-Dimensional Atomic Crystals. *Proc. Natl. Acad. Sci. U. S. A.* **2005**, *102*, 10451−10453.

(20) Alem, N.; Yazyev, O. V.; Kisielowski, C.; Denes, P.; Dahmen, U.; Hartel, P.; Haider, M.; Bischoff, M.; Jiang, B.; Louie, S. G. Probing the Out-of-Plane Distortion of Single Point Defects in Atomically Thin Hexagonal Boron Nitride at the Picometer Scale. *Phys. Rev. Lett.* **2011**, *106*, 126102.

(21) Gibb, A. L.; Alem, N.; Chen, J.-H.; Erickson, K. J.; Ciston, J.; Gautam, A.; Linck, M.; Zettl, A. Atomic Resolution Imaging of Grain Boundary Defects in Monolayer Chemical Vapor Deposition-Grown Hexagonal Boron Nitride. *J. Am. Chem. Soc.* **2013**, *135*, 6758−6761.

(22) Markov, I. V. *Crystal Growth for Beginners: Fundamentals of Nucleation, Crystal Growth, and Epitaxy*, 2nd ed.; World Scientific Publishing Company: River Edge, NJ, 2003.

(23) Chen, L.; Liu, B.; Abbas, A. N.; Ma, Y.; Fang, X.; Liu, Y.; Zhou, C. Screw-Dislocation-Driven Growth of Two-Dimensional Few-Layer and Pyramid-like WSe2 by Sulfur-Assisted Chemical Vapor Deposition. *ACS Nano* **2014**, *8*, 11543.

(24) Zhang, L.; Liu, K.; Wong, A. B.; Kim, J.; Hong, X.; Liu, C.; Cao, T.; Louie, S. G.; Wang, F.; Yang, P. Three-Dimensional Spirals of Atomic Layered MoS2. *Nano Lett.* **2014**, *14*, 6418.

(25) Zhu, J.; Peng, H.; Marshall, A. F.; Barnett, D. M.; Nix, W. D.; Cui, Y. Formation of Chiral Branched Nanowires by the Eshelby Twist. *Nat. Nanotechnol.* **2008**, *3*, 477−481.

(26) Morin, S. A.; Jin, S. Screw Dislocation-Driven Epitaxial Solution Growth of ZnO Nanowires Seeded by Dislocations in GaN Substrates. *Nano Lett.* **2010**, *10*, 3459−3463.

(27) Meng, F.; Morin, S. A.; Forticaux, A.; Jin, S. Screw Dislocation Driven Growth of Nanomaterials. *Acc. Chem. Res.* **2013**, *46*, 1616−1626.

(28) Morin, S. A.; Forticaux, A.; Bierman, M. J.; Jin, S. Screw Dislocation-Driven Growth of Two-Dimensional Nanoplates. *Nano Lett.* **2011**, *11*, 4449−4455.

(29) Zhuang, A.; Li, J.-J.; Wang, Y.-C.; Wen, X.; Lin, Y.; Xiang, B.; Wang, X.; Zeng, J. Screw-Dislocation-Driven Bidirectional Spiral Growth of Bi2Se3 Nanoplates. *Angew. Chem.* **2014**, *126*, 6543−6547.

(30) Mak, K. F.; Lee, C.; Hone, J.; Shan, J.; Heinz, T. F. Atomically Thin MoS2: A New Direct-Gap Semiconductor. *Phys. Rev. Lett.* **2010**, *105*, 136805 .

(31) Splendiani, A.; Sun, L.; Zhang, Y. B.; Li, T. S.; Kim, J.; Chim, C. Y.; Galli, G.; Wang, F. Emerging Photoluminescence in Monolayer MoS2. *Nano Lett.* **2010**, *10*, 1271−1275.

(32) Liu, Z.; Amani, M.; Najmaei, S.; Xu, Q.; Zou, X.; Zhou, W.; Yu, T.; Qiu, C.; Birdwell, A. G.; Crowne, F. J. Strain and Structure Heterogeneity in MoS2 Atomic Layers Grown by Chemical Vapour Deposition. *Nat. Commun.* **2014**, *5*, 5246.

(33) Lu, N.; Guo, H.; Li, L.; Dai, J.; Wang, L.; Mei, W.-N.; Wu, X.; Zeng, X. C. MoS 2/MX 2 Heterobilayers: Bandgap Engineering via

Tensile Strain or External Electrical Field. *Nanoscale* **2014**, *6*, 2879–2886.
(34) Kim, K.; Coh, S.; Tan, L. Z.; Regan, W.; Yuk, J. M.; Chatterjee, E.; Crommie, M. F.; Cohen, M. L.; Louie, S. G.; Zettl, A. Raman Spectroscopy Study of Rotated Double-Layer Graphene: Misorientation-Angle Dependence of Electronic Structure. *Phys. Rev. Lett.* **2012**, *108*, 246103.
(35) Koma, A. Van Der Waals Epitaxy—a New Epitaxial Growth Method for a Highly Lattice-Mismatched System. *Thin Solid Films* **1992**, *216*, 72–76.
(36) Azizi, A.; Eichfeld, S.; Geschwind, G.; Zhang, K.; Jiang, B.; Mukherjee, D.; Hossain, L.; Piasecki, A.; Kabius, B.; Robinson, J. A.; et al. Freestanding van Der Waals Heterostructures of Graphene and Transition Metal Dichalcogenides. *ACS Nano* **2015**, *9*, 4882–4890.
(37) Ji, Q.; Kan, M.; Zhang, Y.; Guo, Y.; Ma, D.; Shi, J.; Sun, Q.; Chen, Q.; Zhang, Y.; Liu, Z. Unravelling Orientation Distribution and Merging Behavior of Monolayer MoS2 Domains on Sapphire. *Nano Lett.* **2015**, *15*, 198–205.
(38) Wang, S.; Wang, X.; Warner, J. H. All Chemical Vapor Deposition Growth of MoS2: H-BN Vertical van Der Waals Heterostructures. *ACS Nano* **2015**, *9*, 5246–5254.

DOI: 10.1021/acs.nanolett.5b01311
Nano Lett. XXXX, XXX, XXX–XXX